JOURNAL OF MATERIALS SCIENCE 13 (1978) 1658–1670

The deformation and fracture of austenitic heat-resisting steel with grain-boundary reaction nodules

MANABU TANAKA
Graduate School, Tokyo Metropolitan University, Tokyo, Japan
TSUNE-AKI SAKAKI, OHMI MIYAGAWA
Faculty of Technology, Tokyo Metropolitan University, Tokyo, Japan

The tensile properties in 21-4N austenitic engine valve steel containing pearlitic nodules due to the grain-boundary reaction have been investigated at room temperature. Some theoretical considerations on the deformation and fracture behaviour of this steel are also presented. In the steel with grain-boundary reaction nodules more than about 10% in area fraction, the ductility decreases considerably with their increase owing to the brittle fracture of rod-like precipitates in the nodules. Although the grain-boundary reaction also decreases the tensile stress and 0.2% proof stress, its effect is more noticeable on ductility than on strength. A theory is developed to explain the work-hardening behaviour as well as the fracture mechanism using a model for composite materials and a good agreement between theoretical and experimental results is obtained.

1. Introduction

In an austenitic engine valve steel with high concentrations of carbon and nitrogen, spherical pearlite nodules with rod-like precipitates are apt to be formed by the grain-boundary reaction as well as intragranular spherical precipitates [1–4]. The authors have been investigating the effect of the grain-boundary reaction on the mechanical properties using a 21-4N engine valve steel. It was found that at elevated temperatures the reaction increases ductility and creep rupture strength has a maximum when the extent of the reaction is about 10% in area fraction, while more than 10% considerably lowers ductility at room temperature [5]. In valve steels, the mechanical properties at room temperature are important as well as those at elevated temperatures. However, the reason why ductility at room temperature decreases owing to the grain-boundary reaction has been unknown.

In this work, the tensile properties of 21-4N austenitic engine valve steel with various amounts of the reaction have been investigated at room temperature. A discussion of the deformation and fracture mechanism of a steel with grain-boundary reaction nodules is then given, based on a composite materials model.

2. Experimental procedure

Commercial 21-4N steel bars, 16 mm in diameter were used in this work. The chemical compositions are given in Table I. Specimens cut out from these bars were solution-heated for 1 h at 1200° C and then water-quenched, furnace-cooled or directly quenched in a furnace maintained at a certain ageing temperature. Subsequent ageing was carried out in the range 700–1000° C in order to obtain specimens of about equal hardness (320 H_v) with various amounts of the reaction and also some of

TABLE I Chemical compositions of the steel used (wt %)

Steel	C	N	Cr	Ni	Mn	Si	S	P	Fe
21-4N	0.51	0.40	20.22	3.90	8.75	0.15	0.008	0.019	bal.

greater hardness ($357\,H_v$). Test pieces, of 50 mm gauge length and 8 mm in diameter, were machined from these specimens. A tensile test was performed to rupture at a constant strain rate of 1.3×10^{-4} sec^{-1} at room temperature (20° C).

The measurement of the extent of the reaction (area fraction) was made by means of linear analysis using a number of optical micrographs. The volume fraction was also calculated from this result. Each volume fraction of rod-like precipitates in the nodules and of intragranular spherical precipitates was determined from a number of transmission electron micrographs of thin films, while the amount of carbon plus nitrogen dissolved in the austenite was estimated from the measurement of the lattice parameter of the austenite with the help of X-ray diffraction.

Ruptured test pieces were cross-sectioned parallel with the longitudinal direction and observed on this side by means of optical microscopy, while initiation of a microcrack was examined by transmission electron microscopy. Further, an investigation was made on the microscopic mode of fracture of the steel with a scanning electron microscope.

In this work, the unreacted and the reacted region are simply denoted by "the matrix" and "the nodules", respectively. Moreover, the grain-boundary reaction is denoted by GBR.

3. Effect of GBR on tensile properties

The relationship between the amount of GBR and the tensile properties at room temperature is shown in Fig. 1. A small amount of GBR has little influence on tensile strength, although more than 60% of it decreases the strength considerably. The 0.2% proof stress decreases with increasing amount of GBR. We shall first discuss the reason for this, because the yield stress is an important factor in the following calculation.

The steel used in this study usually contains spherical or rod-like precipitates in addition to a large amount of dissolved carbon plus nitrogen in austenite in the range 1.0 to 2.3 at.%. Therefore, the yield stress of the steel is considered to be the sum of the precipitation hardening, namely, the contribution of the Orowan stress determined by interparticle spacing, and solid solution hardening due to dissolved carbon plus nitrogen. In general, the Orowan stress on the slip plane is estimated as $\tau_0 \simeq \mu b/l$, where l is the mean interparticle spacing, μ the rigidity of the austenite matrix and b the magnitude of the Burgers vector. The Orowan stress is approximately $\sigma^0_{0N} \simeq 2\,\mu b/l_N$ for the nodules and $\sigma^0_{0M} \simeq 2\,\mu b/l_M$ for the matrix, because the corresponding stress in the tensile direction is about twice as much as this stress. The yield stress of the solid solution without any precipitates is determined only by the solid-solution hardening. In aged specimens the contribution of this to the yield is considered to be given by $\sigma^s_{0N} \simeq \sigma\sqrt{(c_N/c_0)}$ for the nodules and $\sigma^s_{0M} \simeq \sigma\sqrt{(c_M/c_0)}$ for the matrix [6], where σ (431 MPa) is the yield strength of the solid solution, and c_0 (3.91 at.%), c_N and c_M are dissolved carbon plus nitrogen contents in the solid solution, the nodules and the matrix, respectively. Consequently, the yield stress is $\sigma_{0N} \simeq \sigma^0_{0N} + \sigma^s_{0N}$ for the nodules and $\sigma_{0M} \simeq \sigma^0_{0M} + \sigma^s_{0M}$ for the matrix.

Numerical calculations based on the experimental results in Table II show that the contribution of the Orowan stress is almost the same as that of the solution hardening due to dissolved carbon plus nitrogen, and the sum of them is very close to the 0.2% proof stress. In the steel used in this study, the yield stress of the nodules σ_{ON} was always lower than that of the matrix σ_{OM}, because $\sigma^0_{0M} \geqslant \sigma^0_{0N}$ and $\sigma^s_{0M} \geqslant \sigma^s_{0N}$. This is considered to be the most important reason why the 0.2% proof stress decreases with increasing amounts of GBR.

At room temperature more than 10% of GBR considerably decreased ductility. For example, rupture elongation decreases from about 12 to 5% with increasing amount of GBR up to 30% (Fig. 1). A similar relationship is found between reduction of area and amount of GBR. The steel of higher hardness had the lowest ductility in spite of the very small amount of GBR (4%).

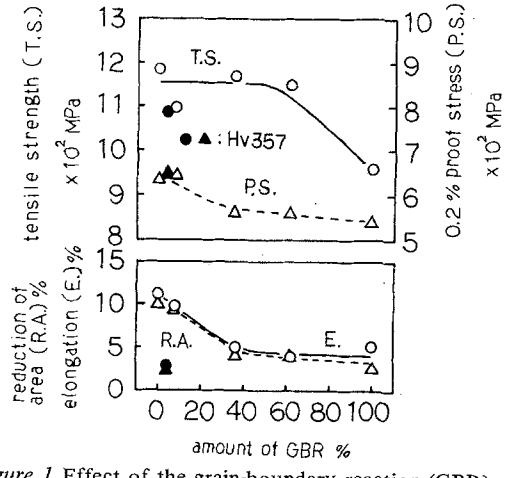

Figure 1 Effect of the grain-boundary reaction (GBR) on the tensile properties.

TABLE II Volume fraction and interparticle spacing of the spherical intragranular precipitates and those of the rod-like precipitates in the GBR nodules

Amount of GBR (%)	Volume fraction of GBR V_N	Spherical intragranular precipitates				Rod-like precipitates in the nodules			
		Interparticle spacing $l_{OM} \times 10^{-7}$ (m)	Mean free spacing $l_M \times 10^{-7}$ (m)	Mean diameter $d_M \times 10^{-7}$ (m)	Volume fraction f_M	Interparticle spacing $l_{ON} \times 10^{-7}$ (m)	Mean free spacing $l_N \times 10^{-7}$ (m)	Mean diameter $d_N \times 10^{-7}$ (m)	Volume fraction f_N
0	0	2.50	1.02	1.48	0.10	–	–	–	–
4 (H_v 357)	0.008	2.61	0.957	1.65	0.064	2.60	1.63	0.97	0.11
8	0.023	2.99	1.53	1.46	0.061	5.50	3.96	1.54	0.061
36	0.216	3.70	1.57	2.13	0.10	3.11	2.00	1.11	0.10
62	0.488	3.51	1.49	2.02	0.072	3.11	2.00	1.11	0.10
100	1.0	–	–	–	–	3.11	2.00	1.11	0.10

4. Microstructures of ruptured specimens

It may be deduced from the foregoing experimental results that there is a close relationship between the decrease in ductility and the change in the fracture mode of the steel owing to occurrence of GBR. Microstructures of ruptured specimens were then examined by means of both optical and electron microscopies. According to scanning electrical microscopy, a facet of a specimen with 0% GBR is an example of a typical intergranular surface, as shown in Fig. 2a. On the contrary, the intergranular surface of a specimen with 36% GBR consists of fine dimples less than 10^{-6} m in diameter (for example, as indicated by arrows in Fig. 2b). By means of optical microscopy, a lot of intergranular cracks could be observed within the GBR nodules near the fracture surface, and these could lead to the rupture of the whole specimen. Further, electron transmission microscopy of this specimen revealed that rod-like precipitates in the nodules contained a lot of these cracks as shown in Fig. 3a. Careful observation with the optical microscope revealed that the frequency of these cracks increased with decreasing orientation difference between the longest axis of rod-like precipitates and the tensile direction, as shown in Fig. 4, while cracks could not be found either in or around the spherical intragranular precipitates at all (Fig. 3b). Therefore, it was considered that at room temperature the brittle fracture of rod-like precipitates in the nodules would lead to the rupture of the whole specimen and would result in a considerable decrease in ductility of specimens with large amounts of GBR.

5. Deformation and fracture of steel with GBR nodules

As schematically shown in Fig. 5, the steel used in this work is a kind of composite material which consists of spherical GBR nodules containing

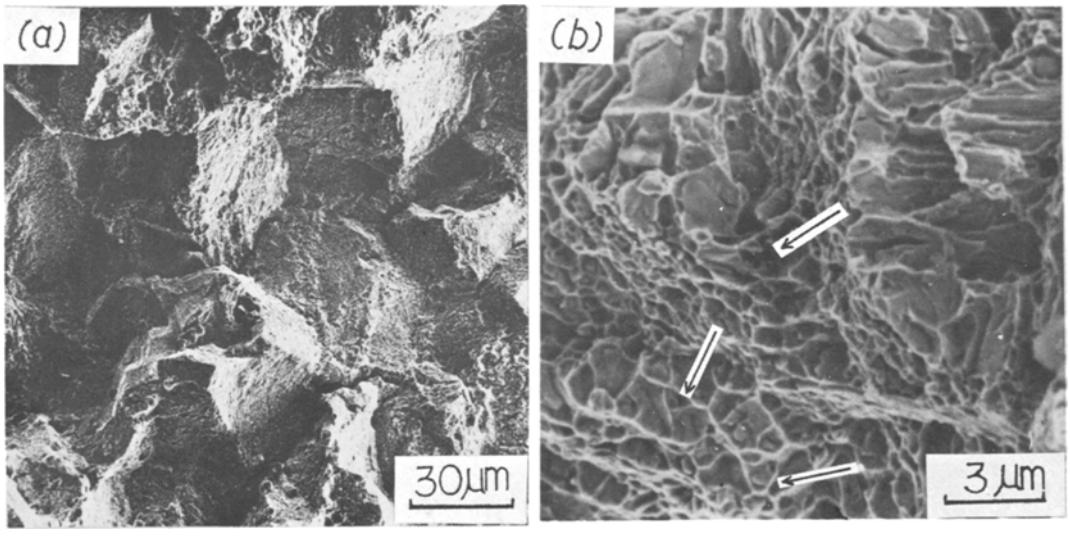

Figure 2 Scanning electron micrographs of tensile ruptured specimens. (a) 0% GBR (b) 36% GBR.

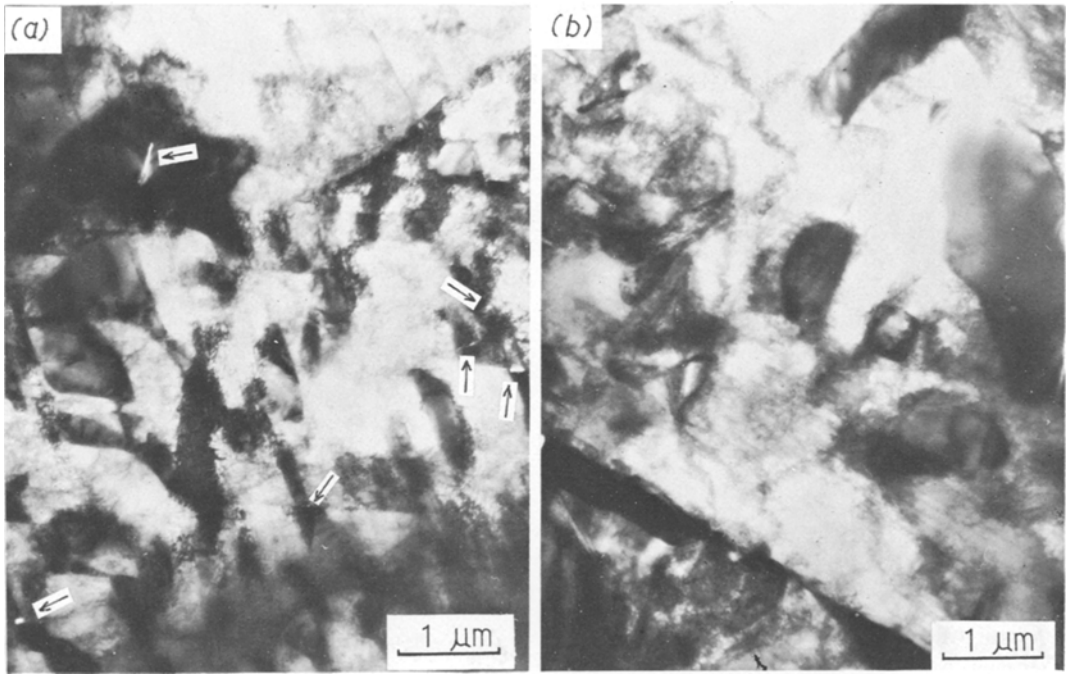

Figure 3 Transmission electron micrographs of tensile ruptured specimen with 36% GBR; (a) cracks in the GBR nodule, (b) intragranular precipitates.

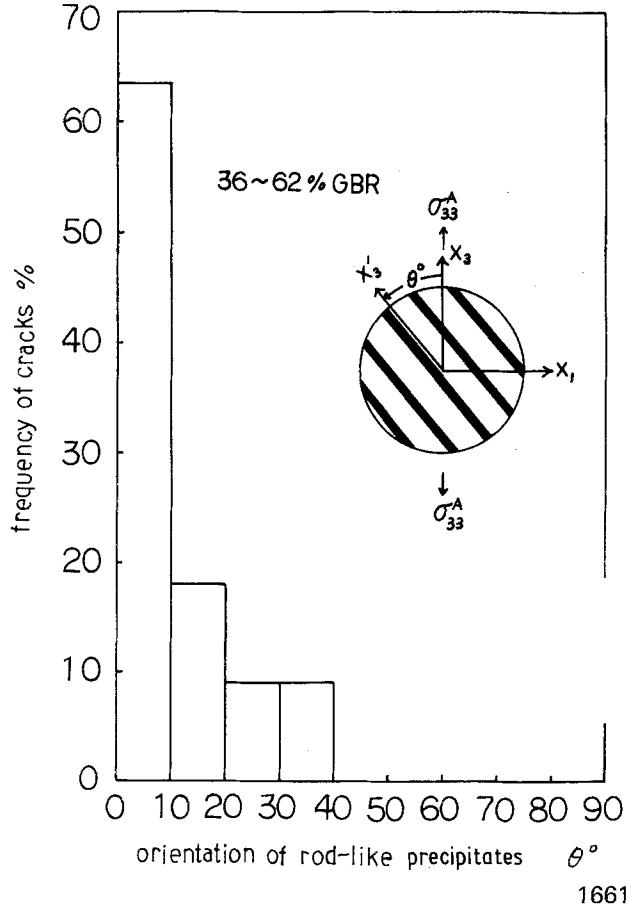

Figure 4 Distribution of the cracks initiated in the rod-like precipitates in the GBR nodules.

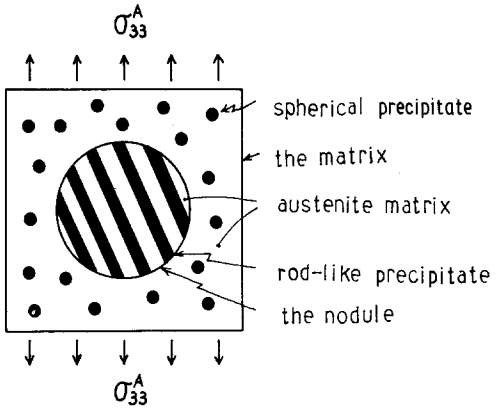

Figure 5 Schematic representation of composite materials in this work.

parallel rod-like precipitates and spherical intergranular $M_{23}C_6$ precipitates. However, the deformation and fracture mechanism of this material has remained unknown so far. We therefore present a theoretical discussion, based on elastic theory, of the mechanism at room temperature.

5.1. Rigidity and Poisson's ratio of $M_{23}C_6$ precipitates and austenite

The rigidity and Poisson's ratio of $M_{23}C_6$ precipitates as well as those of austenite play an important role in the following calculation. Therefore, we begin by considering the rigidity and Poisson's ratio of the steel.

There have been no reports on the experimental values of the rigidity and Poisson's ratio of $M_{23}C_6$ precipitates. However, from the measurement of Young's modulus of the steel in this work, a rigidity $\mu = 8.13 \times 10^4$ MPa and Poisson's ratio $\nu = 0.33$ were obtained for the solid solution without any precipitates, while $\mu = 8.13 \times 10^4$ MPa and $\nu = 0.31$ for the steel with spherical $M_{23}C_6$ precipitates of about 10% in volume fraction. Further, it was found from tensile tests and cold rolling that rod-like precipitates in the nodules would fracture when the total strain of the specimens was in the range 3 to 4%. It is therefore concluded that $M_{23}C_6$ is a material which has the same rigidity and Poisson's ratio as the austenite matrix, and deforms only elastically.

5.2. Elastic strain energy of steel with GBR nodules

Eshelby [7, 8] showed that the internal stresses in the second phase, with eigen-strains and elastic strain energy stored in the material, could be calculated without difficulty when the second-phase particle is ellipsoidal. Further, Tanaka and Mori [9] applied Eshelby's method to the understanding of plastic deformation of a material with non-deforming second-phase particles, and calculated the stress–strain relationship of it. In this work we apply their method in order to discuss the deformation and fracture mechanism of composite materials with GBR nodules.

As shown in Fig. 6, in composite materials, with GBR nodules, plastic deformation occurs only in the austenite of the matrix and that of the nodules under a uniform tensile stress σ_{33}^{A}. A homogeneous plastic strain in the tensile direction is defined by ϵ_{33}^{*} for the matrix and ϵ_{33}^{**} for the nodules, respectively. It is assumed that the plastic strain in each part of the steel is uniform throughout the region and is independent of position. Since a "constant-volume law" holds as regards the plastic deformation, $\epsilon_{33}^{*} = \epsilon^{*}$, $\epsilon_{11}^{*} = \epsilon_{22}^{*} = -\frac{1}{2}\epsilon^{*}$ for the matrix and $\epsilon_{33}^{**} = \epsilon^{**}$, $\epsilon_{11}^{**} = \epsilon_{22}^{**} = -\frac{1}{2}\epsilon^{**}$ for the nodules. Further, an $M_{23}C_6$ particle deforms only elastically, and therefore the average plastic strains amount to $\bar{\epsilon}_{33}^{*} = (1 - f_M)\epsilon^{*}$, $\bar{\epsilon}_{11}^{*} = \bar{\epsilon}_{22}^{*} = -\frac{1}{2}(1 - f_M)\epsilon^{*}$ for the matrix, and $\bar{\epsilon}_{33}^{**} =$

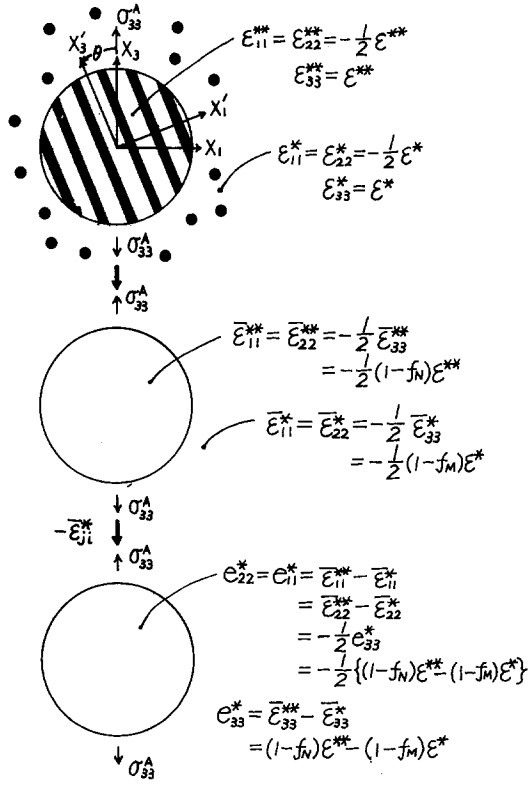

Figure 6 Plastic strains in the nodules and in the matrix.

$(1-f_M)\epsilon^{**}$, $\bar{\epsilon}_{11}^{**} = \bar{\epsilon}_{22}^{**} = -\frac{1}{2}(1-f_N)\epsilon^{**}$ for the nodules, where each volume fraction of the precipitates is f_M for the matrix and f_N for the nodules.

In materials with ellipsoidal non-deforming particles, the internal stress state where the austenite matrix is plastically deformed to plastic strains, ϵ_{ij}, is identical to that when eigen-strains, e_{ij}^T, occur only in the second-phase particles [9]. Constrained strains, e_{ij}^c, are expressed by the Eshelby tensor S_{ijkl} $(i, j, k, l = 1, 2, 3)$ [7] as follows:

$$e_{ij}^c = S_{ijkl} e_{kl}^T. \tag{1}$$

The stresses $\sigma_{ij}^I (i, j = 1, 2, 3)$ in the second-phase particle [6] are

$$\sigma_{ij}^I = \lambda(e^c - e^T)\delta_{ij} + 2\mu(e_{ij}^c - e_{ij}^T) \tag{2}$$

where $e^c = e_{11}^c + e_{22}^c + e_{33}^c$, $e^T = e_{11}^T + e_{22}^T + e_{33}^T$, δ_{ij} is Kronecker's delta and λ Lamé's constant $[= 2\mu\nu/(1-2\nu)]$.

The elastic strain energy of the whole material E (energy stored in matrix and second phase) is as follows:

$$E = -\tfrac{1}{2}\sigma_{ij}^I e_{ij}^T f V \tag{3}$$

where V is volume fraction of the whole material and f that of the second phase.

In the composite materials treated in this work the following three kinds of elastic strain energy can be considered.

(1) E_M, the elastic strain energy stored in the matrix due only to the plastic deformation of the austenite matrix.

(2) E_N, the elastic strain energy stored in the nodules due only to the plastic deformation of the austenite matrix.

(3) E_{MN} the elastic strain energy in the whole material arising from the difference in plastic strain between the nodules and the matrix.

A method of calculating these three kinds of elastic strain energy will be given in the following sections.

5.2.1. E_M, the elastic strain energy stored in the matrix

The internal stresses when the austenite of the matrix is plastically deformed to certain strains, ϵ_{ij}^*, can be calculated according to the foregoing method of Eshelby. Since the superposition of uniform plastic strains has no influence on the stress state, we have only to consider the internal stresses σ_{ij}^{IM} with eigen-strains $e_{ij}^* (= -\epsilon_{ij}^*)$. These stresses are given by

$$\sigma_{11}^{IM} = \sigma_{22}^{IM} = -\frac{7-5\nu}{15(1-\nu)}\mu\epsilon^*$$

$$\sigma_{33}^{IM} = \frac{2(7-5\nu)}{15(1-\nu)}\mu\epsilon^* \tag{4}$$

and the others vanish.

Therefore, the elastic strain energy stored in the matrix, E_M, is given by

$$E_M = \frac{7-5\nu}{10(1-\nu)}\mu\epsilon^{*2} f_M V_M \tag{5}$$

where V_M is volume of the matrix. Further, the interaction energy among the precipitates is neglected here, because stresses outside a precipitate decrease as $(a/r)^3$.

5.2.2. E_N, the elastic strain energy stored in the nodules

The nodules are strengthened by rod-like precipitates aligned in the same direction. The orientation of rod-like precipitates is different in each module. If θ is the orientation difference between the longest axis of those precipitates (x_3'-direction) and the tensile (x_3-direction) (Fig. 6), and if the precipitates have eigen-strains $e_{33}^{**} = -\epsilon^{**}$, $e_{11}^{**} = e_{22}^{**} = \frac{1}{2}\epsilon^{**}$ in (x_1, x_2, x_3) coordinates, those in (x_1', x_2', x_3') coordinates are as follows.

$$e_{11}^{**\prime} = (\tfrac{1}{2}\cos^2\theta - \sin^2\theta)\epsilon^{**}$$

$$e_{22}^{**\prime} = \tfrac{1}{2}\epsilon^{**}$$

$$e_{33}^{**\prime} = (\tfrac{1}{2}\sin^2\theta - \cos^2\theta)$$

$$e_{31}^{**\prime} = e_{13}^{**\prime} = -\tfrac{3}{2}\sin\theta\cos\theta\epsilon^{**} \tag{6}$$

and the others vanish.

The internal stresses σ_{ij}^{IN} in a rod-like precipitate also can be calculated by using the Eshelby tensor [7]. The $\sigma_{ij}^{IN'}$, these stresses in (x_1', x_2', x_3') coordinates are given by

$$\sigma_{11}^{IN'} = \frac{\mu\epsilon^{**}}{8(1-\nu)} \times$$

$$[-(3-8\nu)\cos^2\theta + 2(3-2\nu)\sin^2\theta - 1]$$

$$\sigma_{22}^{IN'} = \frac{\mu\epsilon^{**}}{8(1-\nu)} \times$$

$$[-(1-8\nu)\cos^2\theta + 2(1-2\nu)\sin^2\theta - 3]$$

$$\sigma_{33}^{IN'} = \frac{\mu\epsilon^{**}}{2(1-\nu)} \times$$
$$[(4-\nu)\cos^2\theta - 2(1-\nu)\sin^2\theta - \nu]$$
$$\sigma_{31}^{IN'} = \sigma_{13}^{IN'} = \tfrac{3}{2}\sin\theta\cos\theta\epsilon^{**} \quad (7)$$

and the others vanish.

Consequently, E_N is a function of θ and is expressed by the following equation:

$$E_N = \frac{\mu\epsilon^{**2}}{32(1-\nu)} \times$$
$$[27\cos^4\theta - 6(1+4\nu)\cos^2\theta + 19 - 8\nu]\, f_N V_N \quad (8)$$

where V_N is the volume of the nodules. Again, the interaction energy among these precipitates is neglected.

5.2.3. E_{MN}, the elastic strain energy arising from the difference in the plastic strains between the nodules and the matrix

Since the shape of the precipitates in the nodule is different from that in the matrix, the plastic strain of the former is considered to be different from that of the latter. Therefore, internal stresses, σ_{ij}^{II}, arise from the difference in the average plastic strains between the nodules ($\bar{\epsilon}_{ij}^{**}$) and the matrix ($\bar{\epsilon}_{ij}^{*}$). Putting e_{ij}^{T} as follows

$$e_{33}^{T} = \bar{\epsilon}_{33}^{**} - \bar{\epsilon}_{33}^{*} = (1-f_N)\epsilon_{33}^{**} - (1-f_M)\epsilon_{33}^{*}$$
$$= (1-f_N)\epsilon^{**} - (1-f_M)\epsilon^{*}$$
$$e_{22}^{T} = e_{11}^{T} = \bar{\epsilon}_{11}^{**} - \bar{\epsilon}_{11}^{*}$$
$$= -\tfrac{1}{2}[(1-f_N)\epsilon^{**} - (1-f_M)\epsilon^{*}] \quad (9)$$

then the σ_{ij}^{II} values in a spherical nodule are given by

$$\sigma_{11}^{II} = \sigma_{22}^{II} = \frac{7-5\nu}{15(1-\nu)} \times$$
$$\mu[(1-f_N)\epsilon^{**} - (1-f_M)\epsilon^{*}]$$
$$\sigma_{33}^{II} = -\frac{2(7-5\nu)}{15(1-\nu)}\mu[(1-f_N)\epsilon^{**} - (1-f_M)\epsilon^{*}] \quad (10)$$

and the others vanish.

The elastic strain energy stored in the nodule and matrix, E_{MN} is given by

$$E_{MN} = \frac{7-5\nu}{10(1-\nu)} \times$$
$$\mu[(1-f_N)\epsilon^{**} - (1-f_M)\epsilon^{*}]^2 V_N. \quad (11)$$

5.3. Determination of total free energy, ϵ^* and ϵ^{**}

In the discussion on the deformation behaviour of the steel with the GBR nodules, the following energies should be taken into account as well as the three kinds of energies mentioned above.

The decrease of the external potential in the material, E_{pot} [9], produced by the occurrence of plastic strain under a tensile stress, which is the sum of E_{pot}^{N} due to the nodules and E_{pot}^{M} due to the matrix, is given by

$$E_{pot} = E_{pot}^{M} + E_{pot}^{N}$$
$$= -\sigma_{33}^{A}[(1-f_M)\epsilon^{*}V_M + (1-f_N)\epsilon^{**}V_N]. \quad (12)$$

The energy dissipation occurring during the plastic deformation in the steel, E_{disp} [9], is also the sum of E_{disp}^{N} for the nodules and E_{disp}^{M} for the matrix.

$$E_{disp} = E_{disp}^{M} + E_{disp}^{N}$$
$$= \sigma_{0M}V_M\epsilon^{*} + \sigma_{0N}V_N\epsilon^{**} \quad (13)$$

where the yield stress is σ_{0M} for the matrix and σ_{ON} for the nodules, which is assumed to be the sum of the contribution of the Orowan stress and that of the solid solution hardening.

The free energy change due to the applied stress alone when the steel is homogeneous and has no inclusions is given by

$$E_{elas} = -\frac{1}{2}\frac{(\sigma_{33}^{A})^2}{E} \quad (14)$$

Therefore, the Gibbs free energy of the whole specimen, E_t, is also given by

$$E_t = E_M + E_N + E_{MN} + E_{pot} + E_{disp} + E_{elas}$$
$$= \frac{7-5\nu}{10(1-\nu)}\mu\epsilon^{*2}V_M f_M + \frac{\mu\epsilon^{**2}}{32(1-\nu)}$$
$$[27\cos^4\theta - 6(1+4\nu)\cos^2\theta$$
$$+ 19 - 8\nu]\, V_N f_N$$

$$+\frac{7-5\nu}{10(1-\nu)}\mu[(1-f_N)\epsilon^{**}-(1-f_M)\epsilon^*]^2$$

$$V_N-\sigma_{33}^A[(1-f_M)\epsilon^*V_M+(1-f_N)\epsilon^{**}V_N]$$

$$+(\sigma_{0M}V_M\epsilon^*+\sigma_{0N}V_N\epsilon^{**})-\tfrac{1}{2}(\sigma_{33}^{A2}/E). \quad (15)$$

As already mentioned, the orientation of the rod-like precipitates is different within each nodule. Taking this into account by averaging E_t with respect to θ, the true Gibbs free energy of the steel, $\bar{E}_t$, is given by

$$\bar{E}_t = E_M + E_{pot}^M + E_{disp}^M + \int_0^{\frac{\pi}{2}}(E_N + E_{MN} + E_{pot}^N + E_{disp}^N)\sin\theta\,d\theta + E_{elas} \quad (16)$$

where the plastic strain ϵ^* in the matrix which is a function of an external stress σ_{33}^A and V_M, is independent of position and θ, while the plastic strain ϵ^{**} is a function of σ_{33}^A, V_N and θ.

Hitherto ϵ^* and ϵ^{**} have been treated as unknown quantities, but we next calculate their values. Tanaka and Mori [9] showed that the stress–strain relation of the material with second-phase particles could be calculated by minimizing the Gibbs free energy of the system. Since the steel in this work contains two kinds of precipitates, namely, the GBR nodules with rod-like precipitates and spherical intragranular precipitates, the condition which would minimize the Gibbs free energy should be introduced by the calculus of variations. Therefore, the minimum value of $\bar{E}_t$ is given by ϵ^* and ϵ^{**} which were determined by $\partial\bar{E}_t/\partial\epsilon^* = 0$ and $\partial\bar{E}_t/\partial\epsilon^{**} = 0$

ϵ^* for the matrix is given by

$$\epsilon^* = \frac{1}{2\mu}\frac{(1-f_M)\left[\left(\sigma_{33}^A-\frac{\sigma_{0M}}{1-f_M}\right)V_M + I(\bar{a},\bar{b})(1-f_N)^2\left(\sigma_{33}^A-\frac{\sigma_{0N}}{1-f_N}\right)\frac{16(7-5\nu)}{135f_N}V_N\right]}{\frac{7-5\nu}{10(1-\nu)}\left\{[(1-f_M)^2V_N+f_MV_M]-I(\bar{a},\bar{b})(1-f_M)^2(1-f_N)^2\frac{16(7-5\nu)}{135f_N}V_N\right\}} \quad (17)$$

where

$$\bar{a} = \sqrt{\left\{\frac{2(1+4\nu)}{9}+2\sqrt{\left[\frac{19-8\nu}{27}+\frac{16(7-5\nu)(1-f_N)^2}{135f_N}\right]}\right\}},\ \bar{b} = \sqrt{\left[\frac{19-8\nu}{27}+\frac{16(7-5\nu)(1-f_N)^2}{135f_N}\right]}$$

$$I(\bar{a},\bar{b}) = \frac{1}{4\bar{a}\bar{b}}\log\left|\frac{1+\bar{a}+\bar{b}}{1-\bar{a}+\bar{b}}\right| + \frac{1}{2\bar{b}\sqrt{(4\bar{b}-\bar{a}^2)}}\left[\tan^{-1}\frac{2+\bar{a}}{\sqrt{(4\bar{b}-\bar{a}^2)}}+\tan^{-1}\frac{2-\bar{a}}{\sqrt{(4\bar{b}-\bar{a}^2)}}\right]$$

ϵ^{**} for the nodules is as follows:

$$\epsilon^{**} = \frac{1}{2\mu}\frac{(1-f_N)\left[\sigma_{33}^A-\frac{\sigma_{ON}}{1-f_N}+\frac{7-5\nu}{5(1-\nu)}(1-f_M)\mu\epsilon^*\right]}{\frac{1}{32(1-\nu)}[27\cos^4\theta-6(1+4\nu)\cos^2\theta+19-8\nu]\,f_N+\frac{7-5\nu}{10(1-\nu)}(1-f_N)^2} \quad (18)$$

$\bar{\epsilon}^{**}$, the averaged value of ϵ^{**} with respect to θ is given by

$$\bar{\epsilon}^{**} = \int_0^{\frac{\pi}{2}}\epsilon^{**}\sin\theta\,d\theta = \frac{1}{2\mu}\frac{(1-f_N)\left[\sigma_{33}^A-\frac{\sigma_{ON}}{1-f_N}+\frac{7-5\nu}{5(1-\nu)}(1-f_M)\mu\epsilon^*\right]}{27f_N/[32(1-\nu)]}I(\bar{a},\bar{b}). \quad (19)$$

Consequently, the plastic strain occurring in the whole specimen, ϵ, is as follows.

$$\epsilon = \frac{(1-f_M)V_M\epsilon^* + (1-f_N)V_N\epsilon^{**}}{V_M + V_N}. \quad (30)$$

The stress–strain curves calculated from the above equation and those obtained from the experimental results are shown in Fig. 7. An excellent agreement between the prediction of the present calculations and the experimental results is found within 2% of the plastic strain. As regards the dependence of ϵ^{**} on θ, the minimum value of ϵ^{**} and the highest work hardening rate are predicted when $\theta = 0$, since ϵ^* is greater than ϵ^{**}. The work hardening rate of the nodules is lower than that of the matrix when θ is close to 90°. However, it is obvious that the work hardening rate of the whole material does not increase so much with increasing amount of GBR, as shown in Fig. 7.

5.4. Fracture of material with GBR nodules

It was deduced from microscopic observations that the fracture of rod-like precipitates in the nodules would result in a decrease in the ductility of the material. We now discuss the fracture mechanism of a steel with GBR nodules.

The fracture of a precipitate without pre-existing cracks is predicted to occur when the following two conditions are satisfied.

(1) The tensile stress in a precipitate exceeds its theoretical breaking stress.

(2) The free energy decreases owing to the initiation of a crack.

There are three kinds of stresses in the rod-like precipitates in the nodules. These are a uniformly applied external stress, σ_{ij}^{A}, the internal stresses arising from the difference in the plastic strains between the nodules and the matrix, σ_{ij}^{II} (Equation 10), and those induced by the plastic deformation of the austenite matrix in the nodules (Equation 7). Normal stress σ'_{33} and shear stress σ'_{13} in the x'_3 direction of (x'_1, x'_2, x'_3) coordinates are given by

$$\begin{aligned}\sigma'_{33} &= \sigma_{33}^{II} + \sigma_{33}^{A} + (\sigma_{11}^{II} - \sigma_{33}^{II} - \sigma_{33}^{A}) \\ &\quad \sin^2\theta + \sigma_{33}^{IN'}. \\ \sigma'_{13} &= -(\sigma_{11}^{II} - \sigma_{33}^{II} - \sigma_{33}^{A}) \\ &\quad \sin\theta\cos\theta + \sigma_{13}^{IN'}. \end{aligned} \quad (21)$$

Both the normal stress σ'_{33} and the shear stress σ'_{13} were calculated for a steel with 8% GBR ($f_M = f_N = 0.061$) and that with 36% GBR ($f_M = f_N = 0.10$), when a σ_{33}^{A} corresponding to the tensile strength was applied. The calculations were also made for $f_M = f_N = 0.10$ in the steel with 8% GBR. Those results are shown in Fig. 8. The normal stress σ'_{33} is a maximum when the longest axis of the rod-like precipitates are parallel to the tensile direction ($\theta = 0$), and is about 1.02×10^4 MPa for the steel with 36% GBR. In general, the theoretical breaking stress σ_{max} of the material is in the range 5 to 16% of its Young's modulus [10]. Taking this into account, the calculated values are very close to the theoretical one ($\sigma_{max} \simeq E/20 = 1.08 \times 10^4$ MPa). In the steel with 8% GBR the normal stress increases from about 9.11×10^3 MPa to about 1.54×10^4 MPa with decreasing $f(= f_M = f_N)$ from 0.10 to 0.061. However, it is revealed in any case that the stress condition is almost satisfied for rod-like precipitates when the steel undergoes plastic deformation in the range 3 to 7% with 8% GBR ($f = 0.061$–0.10) and about 4% with 36% GBR under an external stress corresponding to the tensile strength of each steel. A maximum shear stress of about 4.90×10^3 MPa

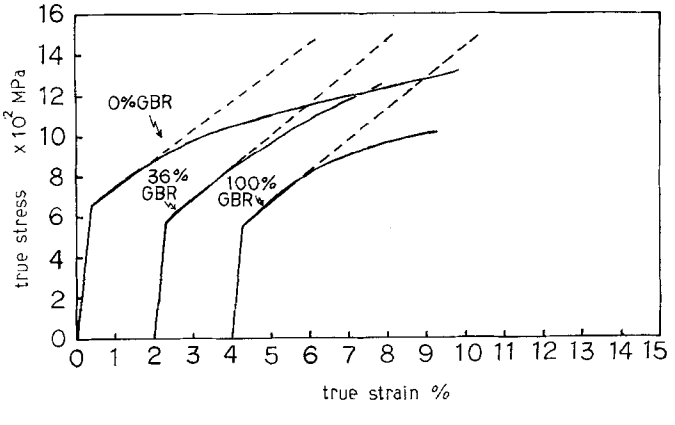

Figure 7 Stress–strain curves obtained from experiment and numerical calculations.

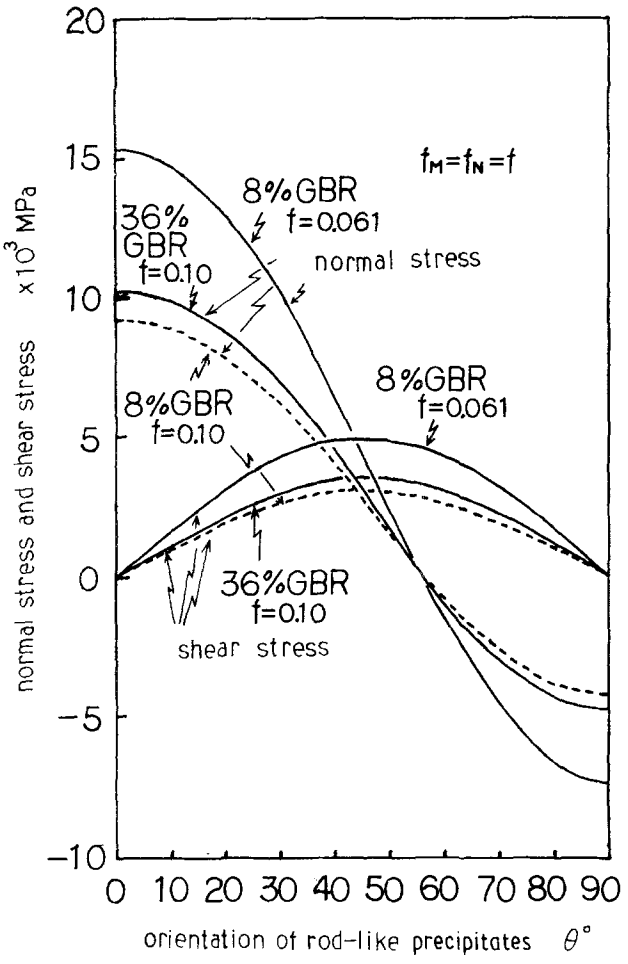

Figure 8 Stresses in rod-like precipitates in the GBR nodules.

is obtained on the steel with 8% GBR for $f = 0.061$ when $\theta = 45°$, but it is still lower than the theoretical shear stress $\tau_{max} = 9.02 \times 10^3$ MPa which is $\frac{1}{9}\mu$ for fcc metals [10]. This implies that no fracture of rod-like precipitates can occur by shear stress alone.

The energy condition for the crack initiation under the action both normal and shear stresses will also be theoretically discussed. The critical size of a crack initiated perpendicularly to the x_3' direction can be calculated by Eshelby's method (see Appendix). In this case the critical radius a is given by

$$a = \frac{3\gamma}{2\left(\sigma_{33}'^2 + \frac{2}{2-\nu}\sigma_{13}'^2\right)\frac{1-\nu}{\pi\mu}} \quad (22)$$

where $\gamma \simeq Ea_0/10$ [10] is the surface free energy, E (2.16×10^5 MPa) is Young's modulus of the steel in this work and a_0 (2.55×10^{-10} m) is the interplanar distance. For instance, the energy condition expressed by Equation 22 is satisfied for a crack radius greater than about 3.70×10^{-8} m in the steel with 36% GBR when $\theta = 0°$. The average radius of the actual rod-like precipitates is approximately 6.00×10^{-8} m, and therefore the energy condition is sufficiently satisfied. The same conclusion was obtained on the steel with 8% GBR. Consequently, it can be considered that the initiation of the fracture is controlled by the stress condition, namely, by the magnitude of the tensile stress applied to the rod-like precipitates in the longitudinal direction. It was revealed from the experimental results that the frequency of fracture of those precipitates considerably increases as their longest axis approaches the tensile direction (Fig. 4). This supports the foregoing prediction that the fracture of rod-like precipitates occurs owing to tensile stress. Therefore, the fracture of the steel with the GBR nodules is considered to occur in the process as shown in Fig. 9.

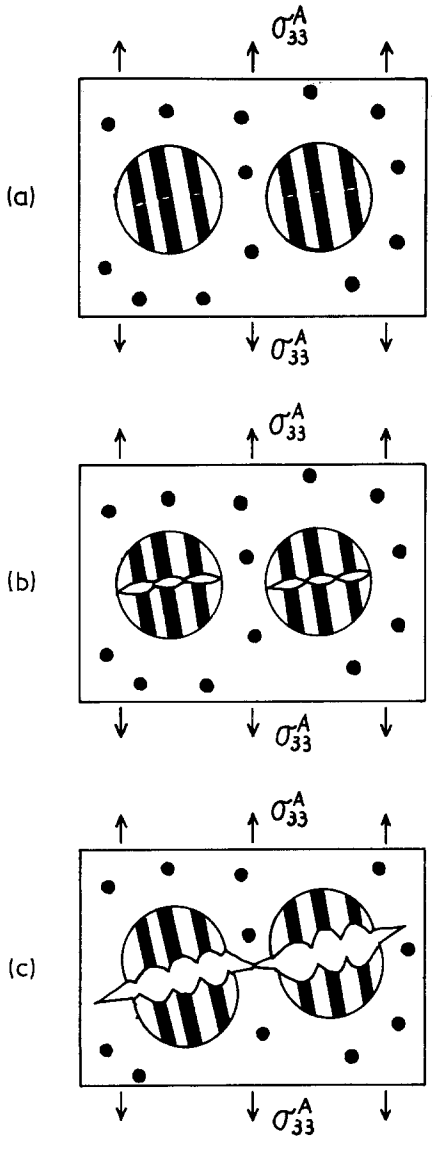

Figure 9 Fracture of the steel with the GBR nodules at room temperature. (a) Initiation at cracks in the nodules. (b) Rupture of the nodules caused by formation of small dimples and their linkage. (c) Rupture of the matrix.

(1) Initiation of microcracks caused by the fracture of rod-like precipitates in the nodules.

(2) A large number of voids formed from these microcracks owing to plastic deformation in the austenite matrix and the fracture of the whole nodule caused by the linkage of these voids.

(3) Intragranular fracture, which results in the rupture of the whole specimen, caused by the propagation of these cracks from the nodules to the adjacent grains.

As for the other materials, the fracture of structural steels with eutectic MnS and those with rod-like MnS [11] is considered to be an example of this type of fracture. However, in the steel with a smaller amount of GBR than 10%, this type of fracture has little effect on the ductility and strength.

However, no cracks in the spherical intragranular precipitates were observed at room temperature. The normal stress in a spherical precipitate in (x_1', x_2', x_3') coordinates, σ_{33}^{M}, is given by

$$\sigma_{33}^{M} = \sigma_{33}^{I} + \sigma_{33}^{A} + \sigma_{33}^{II'} = \sigma_{33}^{I} + \sigma_{33}^{A} - \sigma_{33}^{II} \frac{V_N}{V_M} \tag{23}$$

where $\sigma_{33}^{II'}$ is the "image force" introduced by Eshelby [12] and Brown [13], and is obtained from the relation $\sigma_{ij}^{II'} V_M + \sigma_{ij}^{II} V_N = 0$. $\bar{\sigma}_{ij}^{II}$, the averaged surface traction with respect to θ, is given by the following equation.

$$\sigma_{ij}^{II} = \int_0^{\pi/2} \sigma_{ij}^{II} \sin\theta \, d\theta. \tag{24}$$

Consequently, σ_{33}^{M} is independent of θ, and about 5.40×10^3 MPa for the steel with 36% GBR. In this case, the stress value is too low to satisfy the stress and the energy conditions. This is the important reason why the intragranular precipitates did not fracture, as shown in Fig. 3b.

6. Conclusion

The effect of the grain-boundary reaction (GBR) on the deformation and fracture mechanism of 21-4N engine valve steel has been investigated at room temperature. The results obtained are summarized as follows.

(1) The grain-boundary reaction has a prominent effect on the ductility of the steel. More than 10% of it in the area fraction considerably decreased the ductility.

(2) This is to be attributed to the brittle fracture of rod-like precipitates in the nodules caused by tensile stress, which results in the initiation of the rupture of the whole specimen. This was also predicted by the foregoing theoretical discussion on the fracture of rod-like precipitates.

(3) A small amount of GBR does not have a serious effect on the strength. The decrease in the tensile strength is not very remarkable up to 60% GBR, while the 0.2% proof stress decreases with increasing amount of GBR.

(4) The deformation and fracture mechanism of the steel with both the GBR nodules and intragranular precipitates has hitherto not been under-

stood in detail. In the present work the stress–strain curves and the internal stresses in precipitates, both of the nodules and of the matrix, have been calculated by treating those steels as a kind of composite material. It was shown that agreement between the calculated and the experimental stress–strain relationship was quite good, and the fracture of rod-like precipitates under tensile stress was also explained on this model.

The "composite materials model" used in this work is thought by the authors to be useful not only to explain the deformation and fracture mechanism of this kind of material, but also in discussing the design of composite materials.

Appendix. Initiation and growth of a crack

Conditions for the initiation of a crack in the material are

(1) Stress at the position where the initiation of a crack is predicted exceeds the theoretical breaking stress.

(2) The free energy of the system considered decreases with the initiation of a crack.

There are the following four kinds of energies involved in the free energy of the system, namely, (a) free energy of a crack, (b) work done by external stress according to the crack formation, (c) increase in the surface free energy owing to the crack opening, and (d) sum of the stored elastic energy and the accompanying work done under the uniformly-applied external stress.

The free energy of a crack under stresses, σ_{11}^{A}, σ_{22}^{A}, σ_{33}^{A} and σ_{13}^{A} can be calculated just as before, provided that a crack is penny-shaped $[(x_1^2 + x_2^2)/a^2 + (x_3^2/c^2) = 1, a \gg c]$. The ellipsoidal region is considered to be a crack where the internal stresses, σ_{ij}^{I}, with eigen-strains e_{11}^*, e_{22}^*, e_{33}^* and e_{13}^* in it are compensated by the external stresses σ_{ij}^{A}, namely, $\sigma_{ij}^{I} + \sigma_{ij}^{A} = 0$. Stresses σ_{ij}^{I} with e_{ij}^* are obtained from Equations 1 and 2 in the text. e_{ij}^* are calculated as functions of σ_{ij}^{A} and are given the following equations:

$$e_{11}^* = \frac{\sigma_{11}^{A} - \nu\sigma_{22}^{A}}{2\mu(1+\nu)} - \frac{(1+2\nu)(1-\nu)}{4\mu(1+\nu)}\sigma_{33}^{A}$$

$$e_{22}^* = \frac{-\nu\sigma_{11}^{A} + \sigma_{22}^{A}}{2\mu(1+\nu)} - \frac{(1+2\nu)(1-\nu)}{4\mu(1+\nu)}\sigma_{33}^{A}$$

$$e_{33}^* = \frac{(1+2\nu)(1-\nu)}{4\mu(1+\nu)}(\sigma_{11}^{A} + \sigma_{22}^{A}) - \left[\frac{(9+16\nu)(1-\nu)}{16\mu(1+\nu)} - \frac{2(1-\nu)}{\pi\mu}\frac{a}{c}\right]\sigma_{33}^{A}$$

$$e_{13}^* = \frac{2(1-\nu)}{\pi\mu(2-\nu)}\frac{a}{c}\sigma_{13}^{A} \qquad \text{(A1)}$$

where μ is the rigidity and ν Poisson's ratio of the material. Consequently, the free energy of a crack E_c is obtained just as in Equation 3 of the text.

$$\begin{aligned} E_c &= -\tfrac{1}{2}\sigma_{ij}^{I}e_{ij}^*V = \tfrac{1}{2}\sigma_{ij}^{A}e_{ij}^*V \\ &= \frac{1}{2}\left\{\frac{\sigma_{11}^{A^2} + \sigma_{22}^{A^2} - 2\nu\sigma_{11}^{A}\sigma_{22}^{A}}{2\mu(1+\nu)}\right. \\ &\quad - \frac{(1+2\nu)(1-\nu)}{2\mu(1+\nu)}(\sigma_{11}^{A} + \sigma_{22}^{A})\sigma_{33}^{A} \\ &\quad + \left[\frac{2(1-\nu)}{\pi\mu}\frac{a}{c} - \frac{(9+16\nu)(1-\nu)}{16\mu(1+\nu)}\right]\sigma_{33}^{A2} \\ &\quad \left. - \frac{4(1-\nu)}{\pi\mu(2-\nu)}\frac{a}{c}\sigma_{13}^{A^2}\right\} V. \end{aligned} \qquad \text{(A2)}$$

Since the actual crack is an extemely thin ellipsoid ($c \ll a$), the equation for E_c is simpler, namely,

$$E_c = \frac{1}{2}\left[\frac{2(1-\nu)}{\pi\mu}\sigma_{33}^{A^2} + \frac{4(1-\nu)}{\pi\mu(2-\nu)}\sigma_{13}^{A^2}\right]\frac{a}{c}V \qquad \text{(A3)}$$

where V $(= \frac{4}{3}\pi a^2 c)$ is the volume of a crack. W, the work done on forming the crack is

$$W = -\sigma_{ij}^{A}e_{ij}^*V = -2E_c. \qquad \text{(A4)}$$

The surface free energy of a crack is given by γS (γ is the surface free energy and S the surface area, $S \doteqdot 2\pi a^2$). The sum of the stored elastic energy and the accompanying work done E_0 by external stresses σ_{ij}^{A}, is as follows:

$$E_0 = -\frac{1}{2}\left[\frac{\sigma_{11}^{A^2} + \sigma_{22}^{A^2} + \sigma_{33}^{A^2}}{2\mu(1+\nu)} + \frac{\sigma_{13}^{A^2}}{\mu}\right]V_0 \qquad \text{(A5)}$$

where V_0 is the total volume of the material. G_0 the total free energy of the material with a crack, is given by

$$G = E_c + W + \gamma S + E_0. \qquad \text{(A6)}$$

Conditions 1 and 2 for the initiation of a crack are

$$\sigma_{33}^{A} \geqslant \sigma_{max} \quad \text{or} \quad \sigma_{13}^{A} \geqslant \tau_{max} \qquad (A7)$$

and $G - E_0 = 0$, namely,

$$\sigma_{33}^{A^2} + \frac{2}{2-\nu}\sigma_{13}^{A^2} \geqslant \frac{3}{2}\frac{\pi\mu}{1-\nu}\frac{\gamma}{a} = \frac{3\pi}{10}\frac{1+\nu}{1-\nu}\mu^2\frac{a_0}{a} \qquad (A8)$$

For the steel used in this work, $\sigma_{max} \simeq E/20 = 1.08 \times 10^4$ MPa, $\tau_{max} \simeq \mu/9 = 9.02 \times 10^3$ MPa, and $\gamma = 5.52\,J\,m^{-2}$, since Young's modulus $E = 2.16 \times 10^5$ MPa, Poisson's ratio $\nu = 0.33$ and the interplanar distance $a_0 = 2.55 \times 10^{-10}$ m. Only two components of stress, σ_{33}^{A} and σ_{13}^{A}, are involved in Equation A3, because, for a penny-shaped crack, the terms with σ_{11}^{A} and σ_{22}^{A} are far smaller than those with σ_{33}^{A} and σ_{13}^{A}, and the effect of those stresses on e_{ij}^{*} is negligible.

References

1. M. TANAKA, O. MIYAGAWA, T. SAKAKI and D. FUJISHIRO, *J. Japan Inst. Met.*, **40** (1976) 543.
2. M. KOBAYASHI, M. TANAKA, O. MIYAGAWA, T. SAGA and D. FUJISHIRO, *Tetsu to Haganè* **58** (1972) 1984.
3. M. TANAKA, O. MIYAGAWA and D. FUJISHIRO, *J. Japan Inst. Met.* **38** (1974) 899.
4. M. TANAKA, O. MIYAGAWA and D. FUJISHIRO, *ibid* **41** (1977) 11.
5. M. TANAKA, O. MIYAGAWA, T. SAKAKI and D. FIJISHIRO, Preprint of the 234th Conference at Kansai District, JASME, No. 754-10 (1975) 84.
6. R. HASHIGUCHI and T. CHIKAZUMI, "Strength of Crystals", Series of Materials Science, Asakura **3** (1968) 47.
7. J. D. ESHELBY, *Proc. Roy. Soc.* **A241** (1957) 376.
8. *Idem, ibid* **A252** (1959) 561.
9. K. TANAKA and T. MORI, *Acta. Met.* **18** (1970) 931.
10. A. KELLY, "Strong Solids", (Clarendon Press, Oxford, 1966) 12.
11. I. OYUBI, *Tetsu to Haganè* **61** (1975) 2998.
12. J. D. ESHELBY, *J. Appl. Phys.* **23** (1954) 255.
13. L. M. BROWN and W. M. STOBBS, *Phil. Mag.* **23** (1971) 1185.

Received 16 September and accepted 1 November 1977.